Electronic Supplementary Material (ESI) for Nanoscale.
This journal is © The Royal Society of Chemistry 2016

Superfast and High-Sensitive Printable Strain Sensors with Bioinspired Micronscale Cracks

Honglie Song, Junqiu Zhang, Daobing Chen, Kejun Wang, Shichao Niu, Zhiwu Han* and Luquan Ren

Dr. H. Song, Dr. J. Zhang, Dr. D. Chen, Dr. K. Wang, Dr. S. Niu, Prof. Z. Han, Prof. L. Ren

Key Laboratory of Bionic Engineering (Ministry of Education),

Jilin University,

Changchun 130022, Jilin, P. R. China

E-mail: zwhan@jlu.edu.cn

Table S1 Comparison of the feature sizes of sensing elements and performances of recently reported strain sensors.

Reference	Composite materials	Feature size of sensing elements	Gauge factor[a)]	Response time
[3]	Au NWs	Au NWs ~2 nm in width	7.38	<17 ms
[7]	Ag NWs	NWs ~10 μm in length	14	~3.5 s[b)]
[14]	Ag NWs	Not given	~0.7	~40 ms
[4]	Cr NPs	Nanocrystals ~5 nm in diameter	20	Not given
[12]	Au NPs	NPs ~50 nm in size	70	~10 Hz[b)]
[13]	Au NPs	NPs ~2 and 5 nm in size	40	~1 Hz[b)]
[8]	Pt film	Crack gap ~5 nm in width	>2000	659Hz[b)]
[6]	Pt coated interlocking nanofibers	Nanofibers 50 nm in radius	~11.45	~10 Hz[b)]
[10]	ZnO NWs on PDMS micropillars	ZnO NWs ~50 nm in diameter	Not given	~5 ms
[2]	SWNTs film	SWNTs film ~30 nm in thick	Not given	<10 ms
[5]	SWCNT films	SWCNT films ~400 nm thick	0.82	~14 ms
[9]	CNT fibers	CNT fiber arrays ~250 μm in height	64	~300 ms[b)]
[15]	CNT microyarn	Size as CNT nanofibrils	Not given	63 ms
[1]	Graphite flakes	Cracks and overlaps ~200 nm in width	536.61	~110 ms
[16]	Graphite flakes	Microcracks ~14.7 μm in width	522.6 / 11344	99Hz[b)]
[11]	Crumpled graphene	Not given	7.1	~400 ms[b)]

[a)] The detailed Gauge factor is the maximum sensitivity of the same sensor. [b)] The response time is not explicitly given, and the response time is estimated by the maximum frequency or the minimum time of 1/2 period.

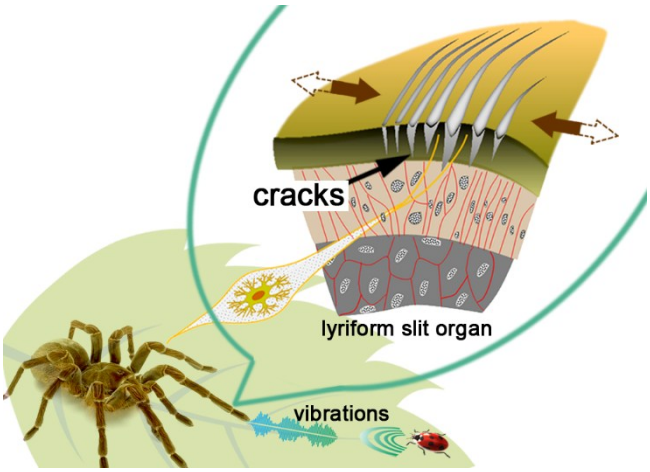

Fig. S1 Schematic of the spiders' sensing minute vibrations with lyriform organ near their leg joints. Micronscale cracks embedded into the exoskeleton of spiders, cutting the lyriform organ into discrete-islands. The lyriform organ responds to mechanical disturbance by converting vibration stimulus into deformation of the lyriform organ (represented by the gray arrows).

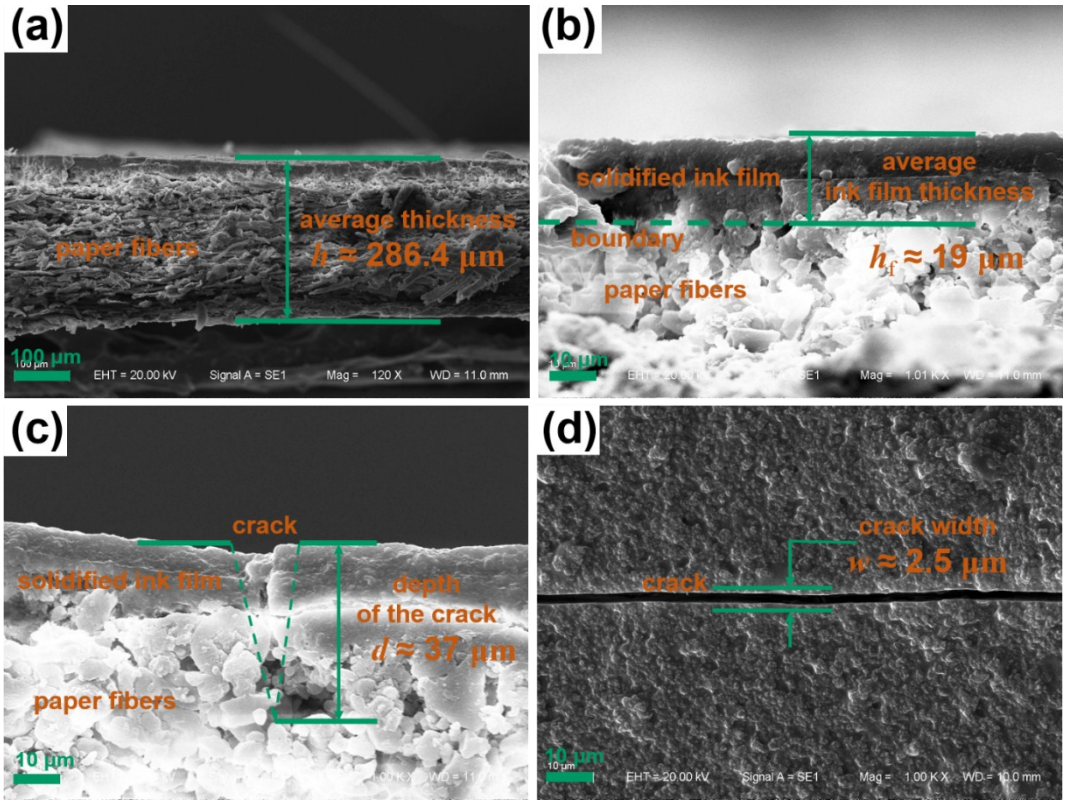

Fig. S2 Cross-sectional SEM images of the cracks. The cross sections were obtained by cutting the sensor along the transverse direction using a scissors after frozen in liquid nitrogen. (a) The average thickness of the sensor h is about 286.4 μm (including the thickness of paper substrate and solidified ink film). (b) The thickness of the solidified ink film h_f is averaged 19 μm. There is an obvious boundary between the solidified ink film and the incompact paper fibers. (c) Cross section of the cracks. The ink partly infiltrated into paper, so that the cracks penetrate ink film into paper fibers. The depth of the crack d is ~37 μm, which is greater than the thickness of the ink film. (d) The width of the crack from surface is about 2.5 μm in relaxing state.

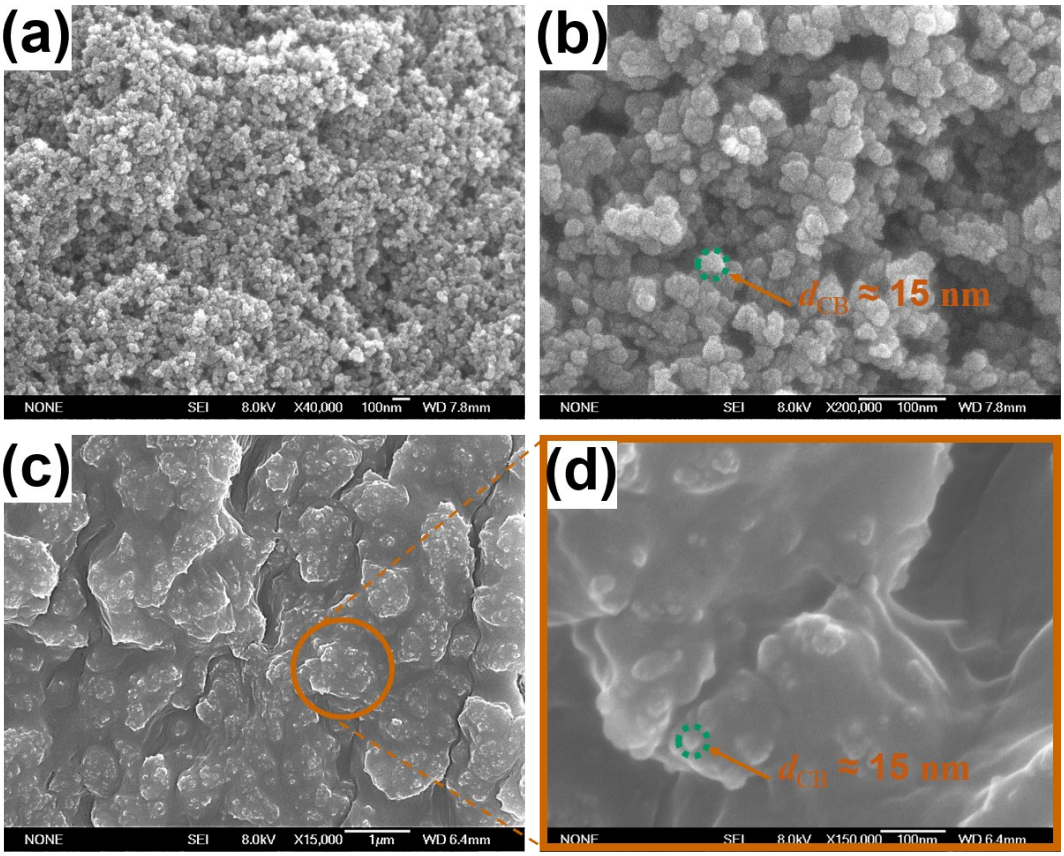

Fig. S3 FESEM images of the carbon black and fracture surfaces of the cracks. (a), (b) As indicated by the FESEM images, the diamater of the CBs used (BLACK PEARLS 2000, Cabot Co.) was about 15 nm, which was consistent with the product description. (c), (d) The morphology of the CB particles embeding into the fracture surfaces of cracks. Each single CB particle dispersed in the ink film retained its original size. The 15 nm particle size, which is sufficient for the possibility of numerous CB-CB junctions and electrons can pass through the CB junctions.

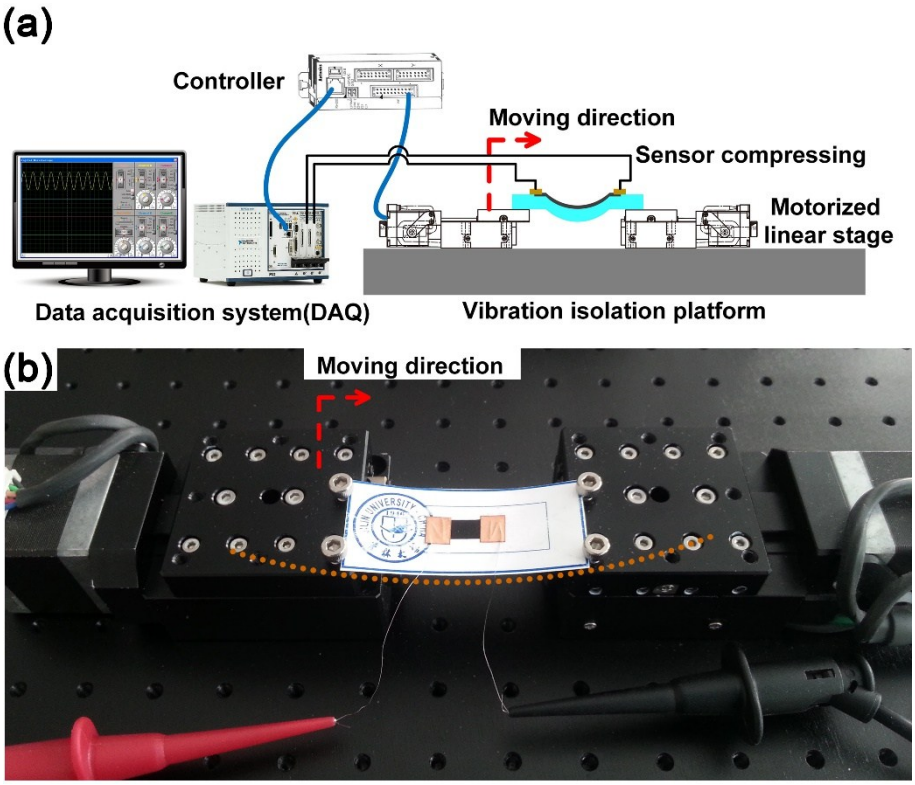

Fig. S4 Schematic illustration and picture of the experimental set-up for evaluation of gauge factor (GF) of the sensor. (a) A home-made experimental set-up is designed to evaluate the resistance response of the as-fabricated sensor to compressive and tensile strain. It contains two positioning controlled motorized linear stages (SURUGA SEIKI) and a data acquisition system (DAQ). The system can provide compression or tension with resistance of the sensor recorded simultaneously. The resistance is measured by a LabVIEW based PXI-4071 system (NI instrument). (b) Picture of test when resistance of the sensor changed under compressive strains.

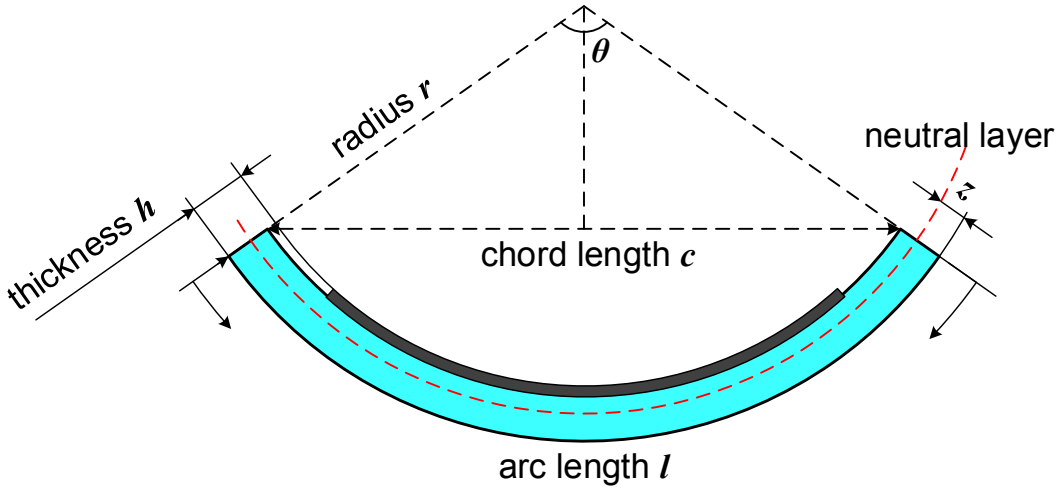

Fig. S5 Deriving the expression of the strain ε. The schematic is the model of the bended sensor when enduring compressive strain. The sensor was tailored to be 21 × 50 mm, with constant arc length l = 50 mm. The sensor was bended with radius r, into chord length c, thickness h, central angle θ, and the distance from bottom surface of the sensor to the neutral layer is z. Relationships between θ, r, c and l can be expressed as:[1]

$$\boldsymbol{\theta} \bullet \boldsymbol{r} = \boldsymbol{l} \qquad \text{eqn (1)}$$

$$\boldsymbol{r} \bullet \sin(\frac{\boldsymbol{\theta}}{2}) = \frac{\boldsymbol{c}}{2} \qquad \text{eqn (2)}$$

When applying compressive strain, the sensor was bended into a certain central angle θ_1 with radius r_1, while the initial were θ_0 and r_0. Therefore, the compression strain $\boldsymbol{\varepsilon}$ can be descirbed as follows:

$$\boldsymbol{\varepsilon} = \frac{\Delta \boldsymbol{l}}{\boldsymbol{l}} = \frac{\boldsymbol{l}_1 - \boldsymbol{l}_0}{\boldsymbol{l}_0} = \frac{\boldsymbol{\theta}_1(\boldsymbol{r}_1 - \boldsymbol{z}) - \boldsymbol{\theta}_0(\boldsymbol{r}_0 - \boldsymbol{z})}{\boldsymbol{\theta}_0(\boldsymbol{r}_0 - \boldsymbol{z})} \qquad \text{eqn (3)}$$

In this process, $\theta_1 \bullet r_1 \approx \theta_0 \bullet r_0$, $r_1 \gg z$ and the initial $r_0 \to \infty$ when the sensor is flat, the eqn (3) can be simplified as:

$$\boldsymbol{\varepsilon} = \frac{\boldsymbol{z}(\boldsymbol{\theta}_0 - \boldsymbol{\theta}_1)}{\boldsymbol{\theta}_0 \boldsymbol{r}_0} = \boldsymbol{z}(\frac{1}{\boldsymbol{r}_0} - \frac{1}{\boldsymbol{r}_1}) = \frac{\boldsymbol{z}}{\boldsymbol{r}_1} \qquad \text{eqn (4)}$$

We suppose that the neutral layer is in the middle of the sensor ($z = h/2$). Subsequently, the compressive strain can be expressed as:

$$\varepsilon = -\frac{h}{2r}$$ eqn (5)

While enduring tensile strain, the situation is similar. The tensile strain can be expressed as:

$$\varepsilon = \frac{h}{2r}$$ eqn (6)

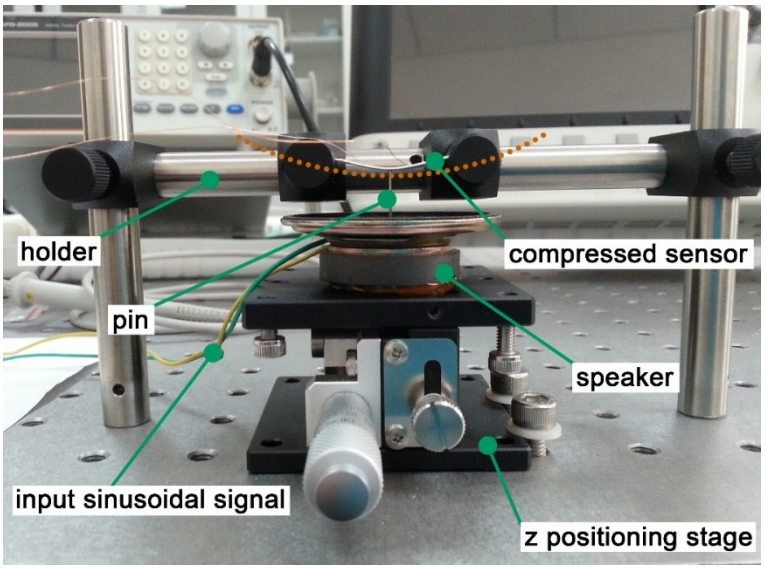

Fig. S6 Picture of the experimental set-up for temporal response of resistance to dynamic mechanical displacements. The initially compressed sensor was fixed to the holder with a pin stuck on the speaker diaphragm hitting the center bottom. The pre-compression is to ensure a reliable contact with the pin both in loading and unloading cycles. External displacements can be exerted by applying sinusoidal signals to the speaker at frequencies of 600, 700 and 800 Hz with a Digital Signal Generator (AFG-2005, GWINSTEK). The resistance variation of the divider resistor (R_0, Fig. 3d) was recorded with an oscilloscope (DSO-X 3032A, Agilent). Then the resistance variation of the sensor was obtained. The displacement of the sensor is simultaneously recorded by a high speed video camera (dimaxHD, PCO) and motion analysis software (TEMA MOTION) for vision-based kinematic recognition. The experimental process also can be seen in Movie S1.

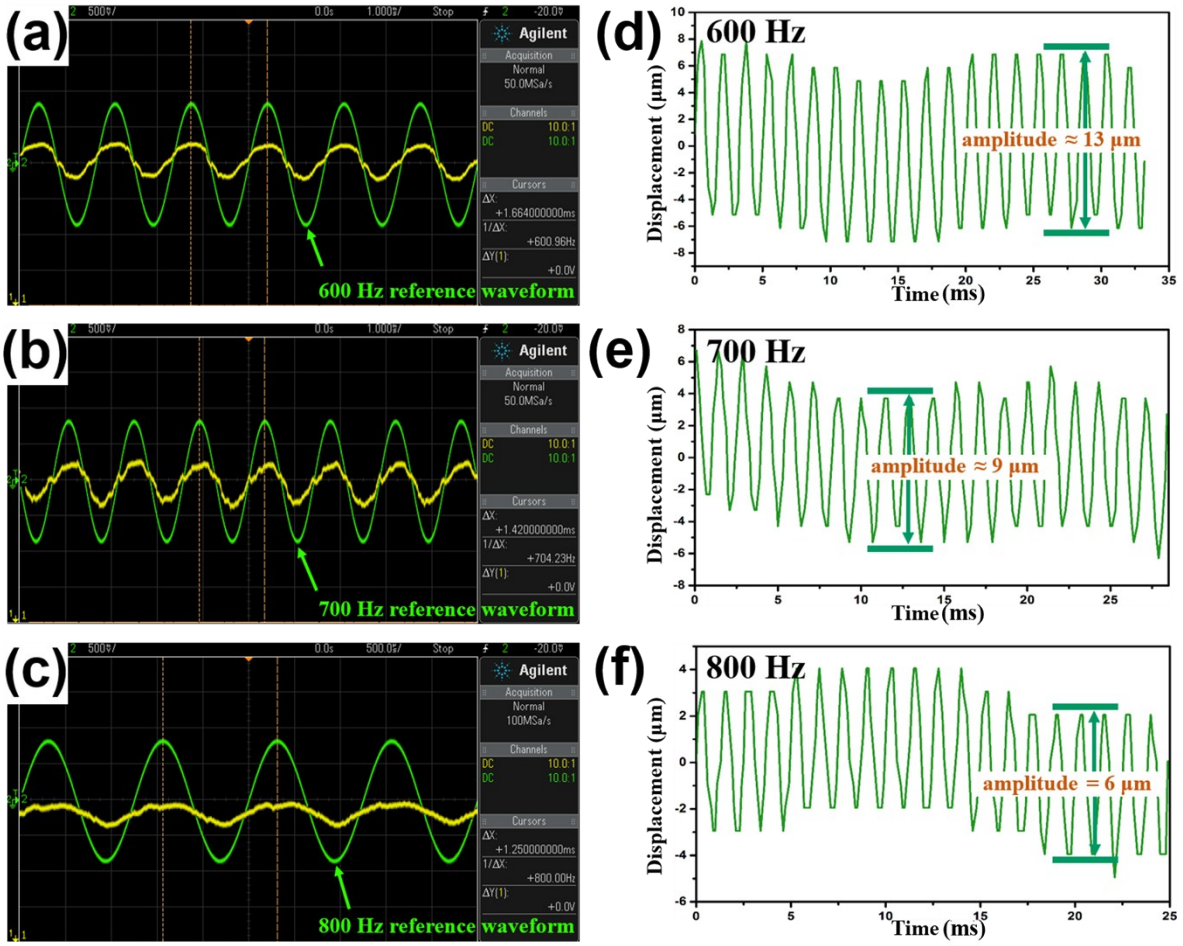

Fig. S7 The resistance of the divider resistor (R_0, as shown in Fig. 3d) and the applied dynamic mechanical displacement. (a), (b) and (c), the resistance variation of R_0 and reference waveforms. The reference sinusoidal signals are at frequencies of 600, 700 and 800 Hz. (d), (e) and (f), the results of kinematic analysis of dynamic mechanical displacement at frequencies of 600, 700 and 800 Hz, which were recorded in real-time by a high speed video camera (dimaxHD, PCO). And TEMA MOTION software was used for vision-based kinematic recognition. The amplitudes of the sinusoidal dynamic mechanical displacement were about 13, 9, and 6 μm, respectively.

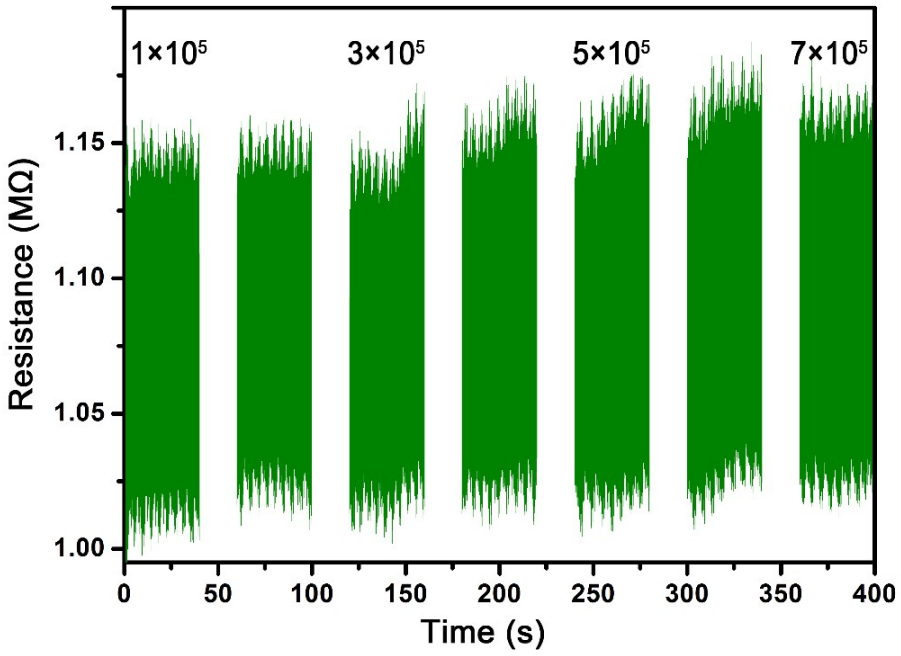

Fig. S8 Durability test of the sensor. To investigate the stability of the sensor, durability test was conduct by applying sinusoidal dynamic mechanical stimuli at 250 Hz. The resistance was recorded during each 10 000 cycles in each 40 s. After 70 000 cycles, the resistance performance of the sensor showed a negligible degradation. It reveals that our strain sensor exhibits high stability, durability and repeatability.

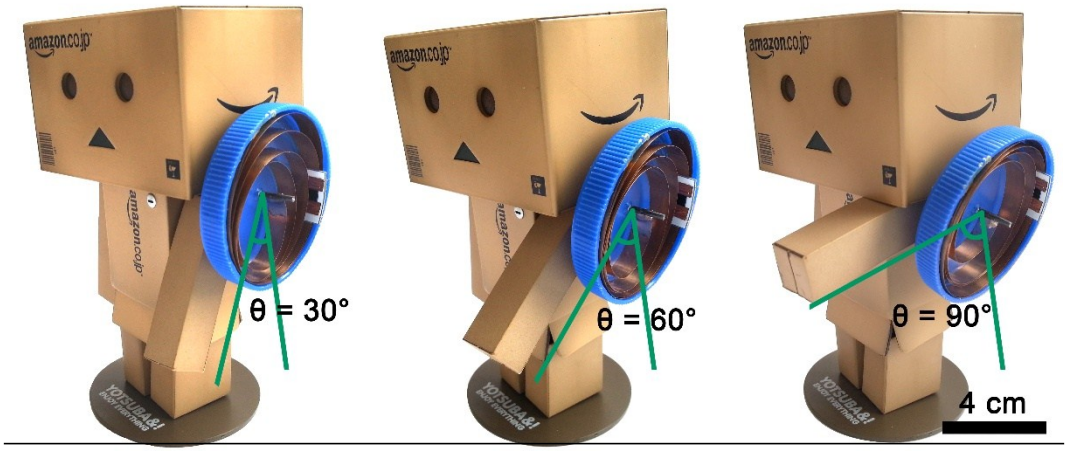

Fig. S9 Demonstration for application as a limited shaft rotation encoder. Pictures of a rotary encoder fixed on the Danbo's shoulder joint for angle measurement.

Movie S1, S2 and S3

Movie S1. Response time to dynamic mechanical stimulus at frequencies of 200, 400, 600, 700 and 800 Hz. In order to investigate the response time of the sensor to dynamic mechanical stimulus, the resistance changes were measured when exerting mechanical displacement at different loading/unloading frequencies at 200, 400, 600, 700 and 800 Hz by the set-up in Fig. S6. A pin fixed on the speaker diaphragm hits the center bottom of the sensor. Displacement were applied to the sensor with the speaker controlled by a digital signal generator. Both the sensor's resistance and the displacement are simultaneously recorded in real-time at different cycling frequencies by oscilloscope and high speed video camera. The tracking ability of our sensor is retained even though the frequency increased to 800 Hz (1.25 ms for each cycle), indicating the superfast response of the sensor. At the end of the movie, the paper substrate is rapidly restored after the stress released.

Movie S2. Demo of vibration detection for human stepping in place. Since the developed PMSCSS has advantages in sensitivity, they can be used to detect the vibrations generated by human stepping in place. With a sensor placed on the near chair, as the person moved, the resistance of the sensor changed instantaneously due to the disturbance of mechanical vibrations transmitted through the ground. A double peak curve was induced by human stepping. In real situations, when the foot off the ground, it will go through two circumstances: when the 1st man lift foot, he shift his weight onto the other foot; while the 2nd man stamp the ground at the moment of lifting off. Correspondingly, for the 1st man, the resistance of the sensor was decreased and increased. While it is vice versa for the 2nd man. And the numbers of steps can be figured out.

Movie S3. Demo of vibration detection for human jumps in place. Jumps can also be detected, as a larger-scale human motion corresponding to a bigger change in resistance of the sensor (~0.3MΩ for steps and ~1MΩ for jumps). Meanwhile, the number of jumps in place can be figured out.

References

[1] X. Liao, Q. Liao, X. Yan, Q. Liang, H. Si, M. Li, H. Wu, S. Cao, Y. Zhang, *Adv. Funct. Mater.,* 2015, **25**, 2395.

[2] X. Wang, Y. Gu, Z. Xiong, Z. Cui, T. Zhang, *Adv. Mater.,* 2014, **26**, 1336.

[3] S. Gong, W. Schwalb, Y. Wang, Y. Chen, Y. Tang, J. Si, B. Shirinzadeh, W. Cheng, *Nat. Commun.,* 2014, **5**, 3132.

[4] M. Zheng, W. Li, M. Xu, N. Xu, P. Chen, M. Han, B. Xie, *Nanoscale,* 2014, **6**, 3930.

[5] T. Yamada, Y. Hayamizu, Y. Yamamoto, Y. Yomogida, A. Izadi-Najafabadi, D. N. Futaba, K. Hata, *Nat. Nanotechnol.,* 2011, **6**, 296.

[6] C. Pang, G.-Y. Lee, T.-i. Kim, S. M. Kim, H. N. Kim, S.-H. Ahn, K.-Y. Suh, *Nat. Mater.,* 2012, **11**, 795.

[7] M. Amjadi, A. Pichitpajongkit, S. Lee, S. Ryu, I. Park, *ACS Nano,* 2014, **8**, 5154.

[8] D. Kang, P. V. Pikhitsa, Y. W. Choi, C. Lee, S. S. Shin, L. Piao, B. Park, K.-Y. Suh, T.-i. Kim, M. Choi, *Nature,* 2014, **516**, 222.

[9] S. Ryu, P. Lee, J. B. Chou, R. Xu, R. Zhao, A. J. Hart, S.-G. Kim, *ACS Nano,* 2015, **9**, 5929.

[10] M. Ha, S. Lim, J. Park, D.-S. Um, Y. Lee, H. Ko, *Adv. Funct. Mater.,* 2015, **25**, 2841.

[11] C. Yan, J. Wang, W. Kang, M. Cui, X. Wang, C. Y. Foo, K. J. Chee, P. S. Lee, *Adv. Mater.,* 2014, **26**, 2022.

[12] W. Jiao, L. Yi, C. Zhang, K. Wu, J. Li, L. Qian, S. Wang, Y. Jiang, B. Das, S. Yuan, *Nanoscale,* 2014, **6**, 13809.

[13] W. Zhao, J. Luo, S. Shan, J. P. Lombardi, Y. Xu, K. Cartwright, S. Lu, M. Poliks, C.-J. Zhong, *Small,* 2015, **11**, 4509.

[14] S. Yao, Y. Zhu, *Nanoscale,* 2014, **6**, 2345.

[15] S. Y. Kim, S. Park, H. W. Park, D. H. Park, Y. Jeong, D. H. Kim, *Adv. Mater.,* 2015, **27**, 4178.

[16] M. Amjadi, M. Turan, C. P. Clementson, M. Sitti, *ACS Appl. Mater. Interfaces,* 2016, **8**, 5618.